THE ASTROPHYSICAL JOURNAL, 287:66–79, 1984 December 1

STELLAR AND GAS KINEMATICS IN DISK GALAXIES

BRADLEY C. WHITMORE[1]
Space Telescope Science Institute; and Department of Terrestrial Magnetism, Carnegie Institution of Washington
AND
VERA C. RUBIN[1] AND W. KENT FORD, JR.
Department of Terrestrial Magnetism, Carnegie Institution of Washington
Received 1983 December 16; accepted 1984 June 19

ABSTRACT

Extended absorption- and emission-line rotation curves and stellar velocity dispersion curves have been obtained for NGC 3898 (Sab), NGC 2841 (Sb), NGC 4062 (Sc), and NGC 2998 (Sc), along with a few observations of NGC 3200 (Sab) and M82 (I). These have been combined with additional observations by Kormendy and Illingworth (1982) to establish the following results. In the disk, the rotation of the gas and stellar components are similar. In the bulge, stellar rotational velocities are only about half of the rotation of the disk. The velocity dispersion curves exhibit a decline with radius, with the small bulge systems showing the steepest decline. A reevaluation of the $V_{\rm bulge}/\sigma_0$ versus ellipticity diagram for spiral bulges shows that models of rotationally flattened oblate spheroids *do not* fully explain the observations.

As part of the analysis, we have performed numerical experiments to determine values of the intrinsic rotation of the bulge in regions where significant fractions of the light come from both the bulge and the disk. These mixing experiments show that differences in both line strengths and velocity dispersions play major roles in producing the observed velocities.

Subject headings: galaxies: internal motions — galaxies: structure

I. INTRODUCTION

Studies of the kinematics of spheroidal star systems have generally been restricted to elliptical galaxies because of their apparent simplicity of form and their high central surface brightness. The few studies of the spheroidal bulge component of spiral galaxies have focused on how bulges compare with elliptical galaxies. However, if our goal is to understand spiral galaxies and the Hubble sequence, we must examine how the bulge, disk, and halo are related. For example, do the bulge and disk have the same angular momentum, and differ only in their velocity dispersions? Is the halo just an extension of the bulge, or is it a separate component? Is a spiral galaxy just an elliptical galaxy with a disk, or are the two fundamentally different?

Kormendy and Illingworth (1982, hereafter KI) conclude that bulges of edge-on spiral and S0 galaxies confirm the predictions of rotating oblate models, unlike large ellipticals, which require anisotropic velocity dispersions. KI studied edge-on systems to avoid the problem of contamination by disk light. Unfortunately, the large optical depth in the disks of these systems makes the determination of an accurate emission-line rotation curve extremely difficult. Therefore, we have chosen to observe less inclined galaxies in order to study both the disk and the bulge.

In § II we determine how the mixture of light from the disk and bulge components affects our observed velocities. In § III we present the data, while in § IV we discuss its implications. A summary is provided in § V.

[1] Visiting Astronomer, Kitt Peak National Observatory, which is operated by the Association of Universities for Research in Astronomy, Inc., under contract with the National Science Foundation.

II. OBSERVATIONS AND REDUCTIONS

We have used the high gain video spectrometer (HGVS) with the Ritchey-Chrétien spectrograph on the 4 m telescope at Kitt Peak Observatory (KPNO) to observe emission and absorption lines in the spectra of spiral galaxies. An observing log is provided in Table 1. A 2.″4 × 3.′2 slit was used with a format of 128 spatial scan lines × 512 wavelength pixels. The wavelength range was from 4700 to 5450 Å, with a spectral resolution of about 3.4 Å FWHM.

Preliminary reductions were performed at KPNO. Details of the HGVS (which incorporates a silicon intensified target, or SIT) and the standard reductions at KPNO are found in KI or in McElroy (1983). Final reductions, including the use of a Fourier quotient technique for measuring absorption-line properties (Sargent *et al.* 1977), were performed at the Department of Terrestrial Magnetism using programs developed within the framework of the Tololo-Vienna reduction system (Ford and Whitmore 1982). This procedure provides measurements of stellar absorption-line velocity dispersion σ, rotational velocity V, and line strength index γ. Rotational velocities for the emission lines were measured separately by using the centroid at half-maximum. An uncalibrated relative line strength was also measured for emission lines, using a continuum which is automatically determined from the pixels adjacent to the emission line. A resolution width (RW) correction of 60 km s^{-1} has been subtracted in quadrature from σ. This correction is needed because low-velocity dispersions are systematically overestimated by the Fourier technique, as found by Whitmore, Kirshner, and Schechter (1979).

Before we compare the dynamics of the bulge and the disk, we must consider three corrections to the data: for beam bending, for the mixture of bulge and disk light, and for projection effects.

TABLE 1

OBSERVING LOG

Object and Axis	Integration (min)	Position Angle (deg)	Date (1981 April)
Galaxies			
NGC 2841:			
Major	40	150	12
Minor	27	60	12
NGC 2998:			
Major	81	53	11
M82:			
Major	17	60	12
NE	14	60	12
SW	14	60	12
NGC 3200:			
Major	40	168	13
NGC 3898:			
Major	20	107	11
NW	34	107	11
Minor	27	17	12
NGC 4062:			
Major	54	108	13
Stars			
HD 127007 (F2 III)	13.5	90	12
HD 134585 (K1 III)	13.5	90	11

NOTE.—The seeing was 2″–3″ on 1981 April 11, 1.″5 on April 12, and 3″ on April 13. Light-to-moderate clouds were present on all three nights. A 2.5 mag neutral density filter was used with the stars.

a) Beam Bending

The stellar velocities near the galaxy nuclei are affected by beam bending for the minor-axis scans of NGC 2841 and NGC 3898 and the major-axis scan of NGC 2841 (Figs. 1 and 2). Beam bending results from building up too much charge on the target of the camera tube of the HGVS before reading it out. The large local charge results in the bending of the readout beam, thus distorting the wavelength scale (see KI for a more detailed description). Fortunately, this effect is easily detected in the folded rotation curve as a separation in the velocities from the two sides of the galaxy. An estimate of the rotational velocities can be made by bisecting the separation. Beam bending appears to have little or no effect on the velocity dispersion.

b) Mixing of Light from the Bulge and the Disk

Decomposition of luminosity profiles shows that in many spiral galaxies both the bulge and the disk contribute to the observed luminosity over a large radius (Kormendy 1977). We have performed numerical experiments for NGC 2841 and NGC 3898 to determine how to decompose the observed velocities and velocity dispersions into the intrinsic values for the bulge and the disk. Photometry comes from Boroson (1981) and from Whitmore and Kirshner (1982).

For the bulge spectrum we use a scan taken near the center where the bulge supplies at least 90% of the total light. The disk spectrum is formed from the addition of several outer scans where the disk dominates. Unfortunately, it is difficult to obtain a spectrum of the disk with good signal-to-noise ratio (S/N) at the larger radial distance where the disk dominates, especially in NGC 3898, an Sab galaxy with a large bulge. However, we find that the relative line strengths of the two components are of primary importance in determining V and σ (as was also found in Whitmore 1980, from similar numerical experiments). Hence a good disk scan can be approximated by using a scan with a value of γ which is lower than the bulge scan. Values of $\gamma_{\rm bulge}/\gamma_{\rm disk}$ between 1.5 and 2.0 are generally found in galaxies such as NGC 2841 and NGC 4062 that have regions dominated by both bulge and disk.

The bulge and disk scans are adjusted to have the same initial S/N by adding Poisson noise to the higher quality bulge scan. The stellar disk velocity, $V_{\rm disk}$, is adopted as the emission-line rotation curve velocity, an assumption that is shown to be true in the outer regions of NGC 4062 and NGC 2998, where the disk dominates. The bulge and disk scans are added together, using the appropriate percentage of light from each component as determined from a decomposition of the luminosity profiles. Poisson noise is again added to degrade the spectrum to a S/N characteristic of the observed spectrum. At each R, the bulge spectrum is shifted in wavelength so that the synthetically summed spectrum produces the observed stellar velocity at that R. The only variable in this procedure is Δ, the velocity difference between the bulge and the disk. We define $V^{\rm los}_{\rm bulge} = V_{\rm disk} + \Delta$ as the intrinsic line-of-sight velocity of the bulge.

The results of our numerical experiments are different from those of McElroy (1983) and Illingworth and Schechter (1982). Given the same ratio of line-strength index, the component with the lower value of the velocity dispersion weights the observed results more strongly (Whitmore 1980). However, McElroy (1983) finds this effect to be much stronger than we do. His results can be attributed to the use of a very high S/N scan of a star for the disk component. When added to a much poorer S/N spectrum for the bulge component, the better quality disk component will dominate the results. For example, in the extreme case when S/N = 0 for the bulge component (a continuum), the disk component will always be found. This is why we have added noise to ensure that the bulge and disk spectrum are of similar quality. Another difference between our studies is that neither McElroy (1983) nor Illingworth and Schechter (1982) consider difference in line strengths between the bulge and disk, an effect which is comparable to or larger than the dispersion effect.

McElroy (1983) was surprised that the rotational velocities in M31 were dominated by the bulge in regions where roughly 30% of the light was from the disk, in contrast to his experiments that indicated that the disk light should dominate the results. Our experiments show that the bulge light should dominate in this region. Figure 3 shows the resultant velocities for three different mixes of velocity dispersions and line strengths, and also McElroy's (1983) results.

c) Correction for Projection Effects

In spheroidal star systems we observe only the projections of the orbital velocities along our line of sight. The observed velocity is therefore lower than the space velocity of the stars. An approximate correction from line-of-sight to space velocities can be made by multiplying the observed velocities by 1.44 (Young *et al.* 1978). This model assumes a flat rotation curve and a constant luminosity gradient of $\ln L/\ln r = -2.3$. Line-of-sight values of the bulge rotation will be denoted $V^{\rm los}_{\rm bulge}$; corrected space velocities are therefore given by

$$V^{\rm space}_{\rm bulge} = (1.44 \csc i) V^{\rm los}_{\rm bulge} .$$

We caution that this correction value is quite uncertain, since the model is unrealistically simple. For example, a line of

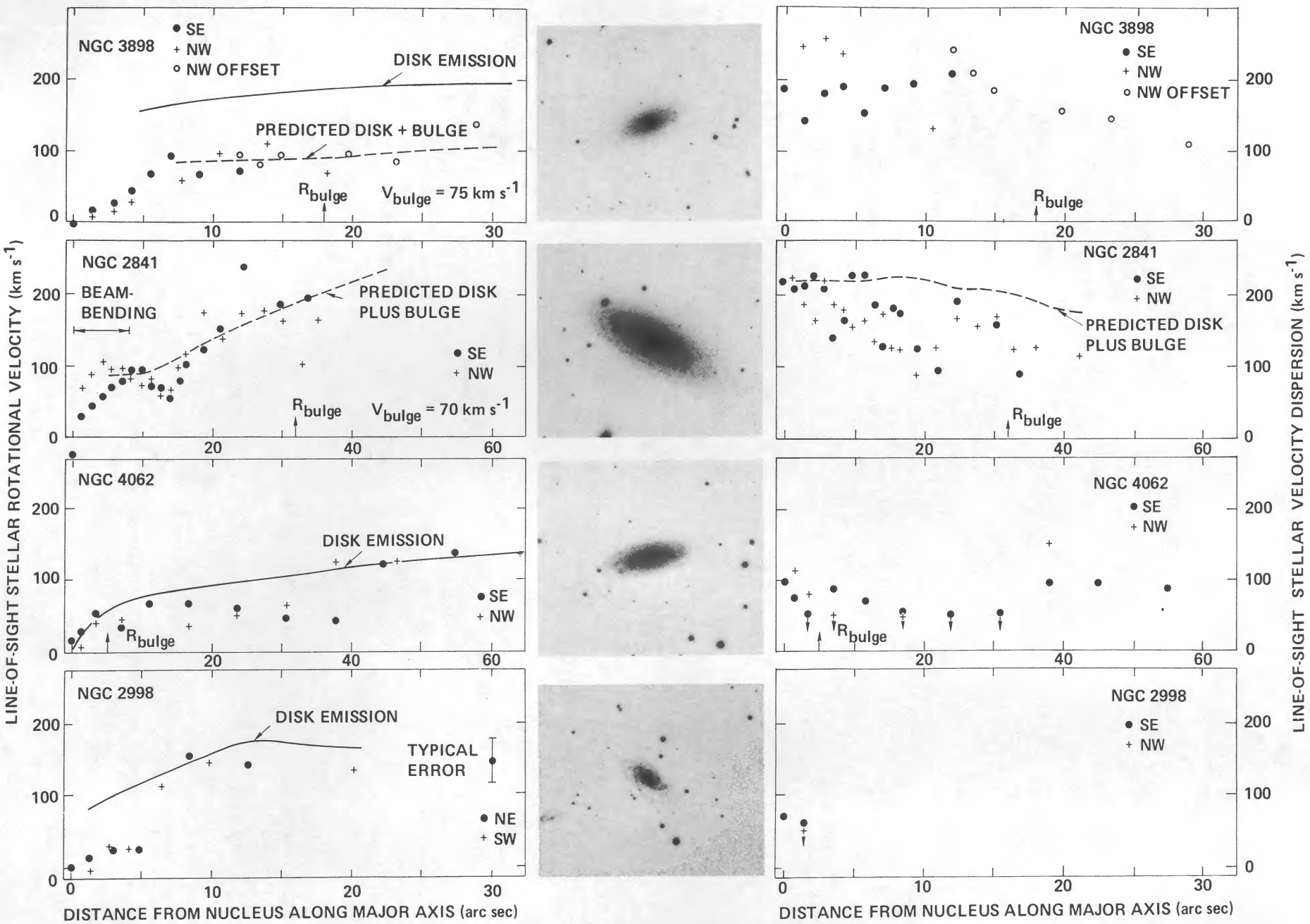

FIG. 1.—(*Left*) Stellar line-of-sight rotational velocities and (*right*) velocity dispersions from absorption lines for the major axis of NGC 3898, NGC 2841, NGC 4062, and NGC 2998. Note how the inner points of the rotation for NGC 2841 are affected by beam bending. Solid lines are the line-of-sight emission-line rotation curves from Rubin, Ford, and Thonnard (1980) and Rubin *et al.* 1984. The dashed lines show velocities predicted by numerical mixing experiments.

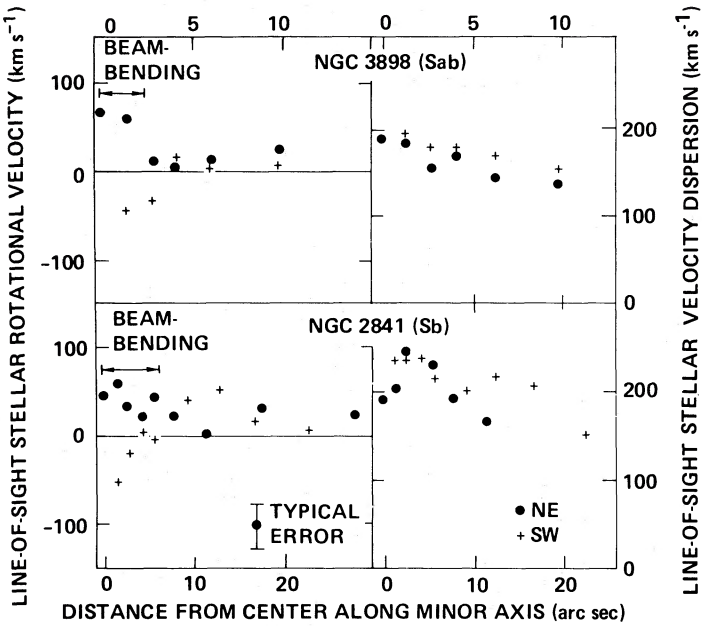

FIG. 2.—Stellar line-of-sight rotational velocities and velocity dispersions from absorption lines for the minor axis of NGC 3898 and NGC 2841. The inner regions of both rotation curves are affected by beam bending.

sight in the outer region samples light from above and below the equatorial plane because the galaxies are not exactly edge-on. KI have shown that rotational velocities are generally smaller above the plane, so our assumption of constant rotational velocities is not accurate. In addition, both the rotational velocities and the luminosity gradient vary with radius, so the correction value should also vary with radius. We estimate that the value of this correction is uncertain by about 20%. Perhaps when more extensive samples are available, it will be possible to handle this complex problem more fully. For the present study, this correction will introduce only a minor uncertainty in the results.

III. RESULTS

The line-of-sight data are presented in Table 2 and in Figures 1 and 2. Comparisons with other measurements (Table 3) indicate that the error estimates from the Fourier quotient program (Table 2) are quite reasonable, with errors of about 10 km s^{-1} in the central velocities, and errors of about 15 km s^{-1} in the central velocity dispersions. For the three galaxies we have in common, our central values of σ are 33% lower than those of Schechter (1983), partly because of the resolution width correction, which we include but Schechter does not. Other possible differences between the two studies arise from the use of different aperture sizes, wavelength regions, template stars, and seeing conditions. If our dispersion measurements are systematically low, our values of $V_{\rm bulge}/\sigma_0$ are systematically high. This would actually strengthen one of the major conclusions of this paper.

The galaxies will be discussed individually. Hubble types come from de Vaucouleurs, de Vaucouleurs, and Corwin (1976), and absolute magnitudes come from Sandage and

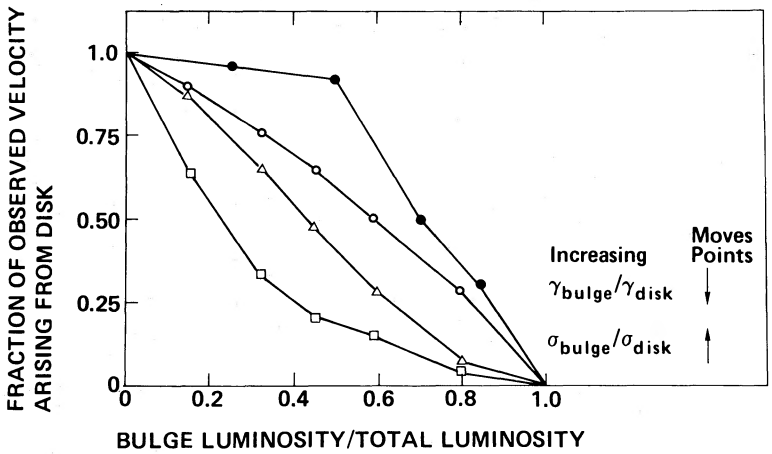

FIG. 3.—Results of numerical mixing experiments showing how the observed rotational velocity shifts from $V_{\rm disk}$ to $V_{\rm bulge}$ as a function of the ratio of the bulge luminosity to the total luminosity. Open circles are for an experiment with values of $(\sigma_{\rm bulge}/\sigma_{\rm disk}, \gamma_{\rm bulge}/\gamma_{\rm disk}) = (1.4, 1.1)$; triangles, (1.8, 2.0); boxes, (3.4, 5.6). The solid dots are from one of McElroy's (1983) experiments. The arrows show the effects of increasing the two ratios.

TABLE 2

ROTATIONAL VELOCITIES, VELOCITY DISPERSIONS, AND LINE-STRENGTH INDICES FROM ABSORPTION LINES

Object	R (n) (arc sec)	cz [a,b] (km/s)	σ [a] (km/s)	Y	V [a,b] (km/s)
NGC 2841 (major axis, Vo=585 km/s)					
	-33.6 (3) SE	779 (24)	87 (29)	0.65 (0.15)	194
	-30.1 (2)	772 (27)	158 (27)	0.79 (0.20)	187
	-24.5 (2)	825 (36)	189 (36)	0.71 (0.24)	240
	-21.7 (2)	738 (24)	93 (27)	0.68 (0.15)	153
	-18.9 (2)	708 (20)	124 (20)	0.84 (0.15)	123
	-16.1 (2)	686 (23)	172 (22)	0.79 (0.17)	101
	-15.4 (1)	664 (26)	179 (25)	0.82 (0.20)	79
	-14.0 (1)	639 (22)	124 (23)	0.69 (0.14)	54
	-12.6 (1)	655 (22)	184 (19)	1.01 (0.19)	70
	-11.2 (1)	657 (16)	224 (15)	1.61 (0.26)	72
	-9.8 (1)	678 (16)	223 (15)	1.44 (0.21)	93
	-8.4 (1)	677 (16)	160 (16)	0.93 (0.15)	92
	-7.0 (1)	[663] (16)	137 (16)	0.73 (0.12)	[78]
	-5.6 (1)	[656] (23)	208 (21)	0.88 (0.19)	[71]
	-4.2 (1)	[644] (20)	224 (18)	1.05 (0.20)	[59]
	-2.8 (1)	[629] (20)	211 (18)	1.00 (0.20)	[44]
	-1.4 (1)	[614] (16)	209 (15)	1.05 (0.18)	[29]
	0.0 (1)	[558] (19)	216 (16)	0.90 (0.17)	[-27]
	1.4 (1)	[515] (20)	221 (18)	0.84 (0.17)	[-70]
	2.8 (1)	[497] (17)	183 (17)	0.82 (0.14)	[-88]
	4.2 (1)	[479] (13)	164 (12)	0.85 (0.10)	[-106]
	5.6 (1)	[491] (16)	219 (14)	1.10 (0.16)	[-94]
	7.0 (1)	[490] (14)	184 (13)	1.08 (0.14)	[-95]
	8.4 (1)	500 (16)	179 (16)	1.01 (0.16)	-85
	9.8 (1)	514 (20)	154 (20)	0.70 (0.13)	-71
	11.2 (1)	512 (18)	163 (17)	0.84 (0.15)	-73
	12.6 (1)	523 (25)	132 (26)	0.70 (0.17)	-62
	14.0 (1)	520 (26)	171 (24)	0.89 (0.21)	-65
	15.4 (1)	488 (25)	124 (28)	0.69 (0.17)	-97
	16.1 (2)	468 (20)	121 (22)	0.78 (0.15)	-117
	18.9 (2)	411 (23)	87 (26)	0.55 (0.12)	-174
	21.7 (2)	446 (27)	124 (29)	0.62 (0.16)	-139
	24.5 (2)	412 (27)	164 (26)	0.79 (0.19)	-173
	27.3 (2)	413 (31)	155 (31)	0.62 (0.18)	-172
	30.1 (2)	424 (31)	167 (32)	0.72 (0.22)	-161
	32.9 (2)	484 (28)	122 (30)	0.66 (0.17)	-101
	35.7 (2)	422 (29)	127 (31)	0.62 (0.17)	-163
	42.0 (2) NW	360 (36)	115 (40)	0.47 (0.16)	-225
NGC 2841 (minor axis, Vo=632 km/s)					
	-28.0 (9) NE	607 (26)	...	1.03 (0.26)	-25
	-17.5 (6)	600 (30)	...	1.48 (0.38)	-32
	11.4 (3)	630 (25)	164 (25)	0.80 (0.19)	-2
	- 7.7 (3)	609 (19)	190 (18)	0.96 (0.18)	-23
	- 5.6 (1)	588 (21)	233 (19)	1.27 (0.25)	-44
	- 4.2 (1)	[610] (20)			[-22]
	- 2.8 (1)	[598] (18)	241 (16)	1.23 (0.20)	[-34]
	- 1.4 (1)	[572] (18)	202 (16)	1.04 (0.18)	[-60]
	0.0 (1)	[584] (17)	190 (16)	0.90 (0.15)	[-48]
	1.4 (1)	[581] (24)	235 (20)	0.92 (0.20)	[-51]
	2.8 (1)	[613] (24)	239 (21)	0.90 (0.20)	[-19]
	4.2 (1)	[639] (27)	235 (24)	0.92 (0.22)	[7]
	5.6 (1)	633 (20)	215 (20)	1.17 (0.23)	-1
	9.1 (2)	675 (24)	200 (22)	0.87 (0.19)	43
	12.6 (3)	687 (23)	218 (21)	1.24 (0.26)	55
	16.8 (3)	649 (33)	202 (32)	0.96 (0.30)	17
	22.4 (5) SW	641 (40)	150 (41)	0.70 (0.27)	9
NGC 2998 (major axis, Vo=4760 km/s)					
	-20.3 (6) NE	4626 (38)	...	...	-134
	-9.8 (3)	4613 (40)	...	...	-147
	-6.3 (2)	4648 (42)	...	0.26 (0.10)	-112
	-4.2 (1)	4737 (37)	...	...	-23
	-2.8 (1)	4732 (21)	...	...	-28
	-1.4 (1)	4764 (26)	<50	0.36 (0.10)	4
	0.0 (1)	4762 (23)	70 (34)	0.37 (0.10)	2
	1.4 (1)	4773 (20)	59 (28)	0.40 (0.09)	13
	2.8 (1)	2787 (30)	...	0.33 (0.10)	27
	4.9 (2)	4784 (33)	...	0.28 (0.09)	24
	8.4 (3)	4914 (41)	...	0.25 (0.11)	154
	12.6 (3) SW	4903 (40)	...	...	143
M82 (major axis, Vo=180 km/s)					
	-120.4 (1) NE [c]	323 (42)	...	...	143
	-113.4 (1)	333 (40)	...	...	153
	-112.0 (1)	320 (35)	...	...	140
	-110.6 (1)	254 (23)	137 (34)	1.18 (0.36)	74
	-107.8 (1)	291 (25)	...	0.87 (0.24)	111
	-102.2 (1)	...	...	1.09 (0.45)	...
	-96.6 (1)	265 (34)	...	...	85
	-95.2 (1)	312 (24)	...	0.86 (0.31)	132
	-82.6 (1)	324 (37)	...	...	144
	-81.2 (1)	349 (24)	...	...	169
	-71.4 (1)	273 (22)	146 (31)	0.98 (0.28)	93
	-70.0 (1)	283 (17)	...	0.89 (0.24)	103
	-68.6 (1)	324 (16)	...	0.88 (0.17)	144
	-65.8 (1)	345 (16)	155 (23)	1.08 (0.22)	165
	-64.4 (1)	349 (11)	142 (25)	1.11 (0.26)	169
	-63.0 (1)	347 (09)	154 (23)	1.45 (0.30)	167
	-61.6 (1)	360 (12)	142 (30)	0.99 (0.27)	180
	-60.2 (1)	377 (21)	...	...	197
	-58.8 (1)	336 (27)	...	...	156
	-56.0 (1)	290 (33)	...	...	110

TABLE 2—*Continued*

Object	R (n) (arc sec)	cz [a,b] (km/s)	σ [a] (km/s)	γ	V [a,b] (km/s)
	-50.4 (1)	...	85 (33)	0.83 (0.18)	...
	-49.0 (1)	310 (41)	...	...	130
	-46.2 (1)	313 (39)	...	...	133
	-44.8 (1)	343 (31)	...	...	163
	-43.4 (1)	333 (33)	...	...	153
	-42.0 (1)	286 (38)	...	...	106
	-36.4 (1)	311 (29)	...	...	131
	-35.0 (1)	...	87 (31)	0.83 (0.19)	...
	-32.2 (1)	...	...	0.75 (0.29)	...
	-1.4 (1)	200 (27)	183 (25)	0.63 (0.16)	20
	0.0 (1)	185 (24)	130 (28)	0.60 (0.14)	5
	1.4 (1)	194 (35)	...	0.43 (0.16)	-14
	14.0 (1)	164 (33)	129 (37)	0.55 (0.19)	16
	19.6 (1)	103 (29)	...	0.47 (0.14)	77
	21.0 (1) SW	126 (29)	...	0.51 (0.14)	54
M82 (major axis, NE scan, Vo=180 km/s)					
	-149.8 (5) NE	316 (33)	113 (35)	0.80 (0.22)	136
	-135.8 (5)	248 (38)	142 (39)	0.83 (0.25)	68
	-130.2 (3)	296 (22)	65 (29)	0.89 (0.17)	116
	-121.8 (3)	337 (27)	66 (34)	0.86 (0.20)	157
	-117.6 (3)	295 (28)	113 (32)	0.93 (0.22)	115
	-113.4 (3)	298 (27)	94 (32)	0.80 (0.19)	118
	-88.2 (3)	335 (35)	...	0.67 (0.20)	155
	-70.0 (1)	317 (25)	...	0.73 (0.17)	137
	-68.6 (1)	313 (38)	136 (38)	0.67 (0.20)	133
	-67.2 (1)	300 (26)	117 (29)	1.00 (0.23)	120
	-65.8 (1)	331 (20)	91 (24)	1.04 (0.19)	151
	-64.4 (1)	354 (32)	184 (30)	1.14 (0.28)	174
	-58.8 (1)	338 (31)	145 (31)	0.91 (0.22)	158
	-57.4 (1)	326 (34)	174 (32)	0.94 (0.24)	146
	-51.8 (1)	337 (38)	...	...	157
	-50.4 (1)	328 (30)	127 (31)	0.88 (0.21)	148
	-49.0 (1)	328 (26)	109 (29)	1.03 (0.21)	148
	-47.6 (1)	346 (23)	119 (24)	1.22 (0.22)	166
M82 (major axis, SW scan, offset 12 arc sec north, Vo=180 km/s)					
	2.8 (1) SW [d]	212 (30)	117 (37)	1.22 (0.36)	32
	13.3 (2)	187 (17)	139 (21)	1.55 (0.38)	7
	21.7 (2)	170 (18)	106 (22)	1.25 (0.32)	-10
	29.4 (1)	118 (26)	126 (29)	1.10 (0.28)	-62
	35.7 (2)	116 (20)	154 (27)	1.51 (0.38)	-64
	53.9 (4)	112 (28)	...	...	-68
	63.7 (2)	136 (27)	139 (40)	0.95 (0.34)	-44
	67.9 (4)	161 (13)	77 (23)	1.10 (0.20)	-19
	97.3 (2)	25 (17)	...	...	-155
	100.1 (2)	54 (14)	160 (26)	1.37 (0.34)	-126
	102.9 (2)	51 (11)	...	...	-129
	105.7 (2)	51 (9)	...	...	-129
	108.5 (2)	70 (14)	...	...	-110
	114.1 (2)	78 (24)	122 (34)	1.13 (0.33)	-102
	116.9 (2)	115 (31)	...	...	-65
	124.6 (3)	89 (32)	137 (39)	1.13 (0.36)	-91
NGC 3200 (major axis)					
	0.7 (6)	3518 (23)	138 (20)	0.75 (0.13)	...
NGC 3898 (major axis, Vo=1175 km/s)					
	-11.9 (4) SE	1247 (38)	210 (36)	0.91 (0.32)	72
	-9.1 (2)	1243 (34)	195 (32)	0.96 (0.34)	68
	-7.0 (1)	1270 (24)	190 (29)	1.04 (0.29)	95
	-5.6 (1)	1243 (22)	154 (25)	0.89 (0.22)	68
	-4.2 (1)	1219 (16)	190 (17)	1.24 (0.22)	44
	-2.8 (1)	1201 (15)	181 (22)	0.92 (0.23)	26
	-1.4 (1)	1188 (15)	143 (19)	0.86 (0.15)	13
	0.0 (1)	1172 (10)	187 (18)	1.00 (0.19)	-3
	1.4 (1)	1165 (20)	247 (16)	1.39 (0.26)	-10
	2.8 (1)	1157 (13)	259 (22)	1.29 (0.30)	-18
	4.2 (1)	1146 (20)	237 (24)	0.99 (0.25)	-29
	7.7 (2)	1116 (38)	...	...	-59
	10.5 (2)	1077 (30)	131 (32)	0.77 (0.22)	-98
	14.0 (3)	1063 (29)	...	...	-112
	18.2 (3) NW	1105 (38)	...	...	-70
NGC 3898 (major axis, NW scan, Vo=1139 km/s)					
	12.0 (1) NW	1042 (27)	242 (23)	1.45 (0.33)	-97
	13.4 (1)	1057 (32)	210 (28)	1.20 (0.32)	-82
	14.8 (1)	1044 (47)	188 (42)	0.78 (0.32)	-95
	19.7 (2)	1041 (27)	159 (28)	1.09 (0.28)	-98
	23.2 (3)	1052 (26)	146 (26)	1.13 (0.28)	-87
	28.8 (5)	1000 (28)	109 (32)	0.73 (0.20)	-139
NGC 3898 (minor axis, Vo=1157 km/s)					
	-9.8 (3) NE	1130 (24)	135 (25)	0.80 (0.18)	-27
	-6.3 (2)	1145 (20)	142 (21)	0.85 (0.16)	-12
	-4.2 (1)	1151 (19)	170 (18)	1.09 (0.20)	-6
	-2.8 (1)	[1144] (14)	154 (14)	1.11 (0.15)	[-13]
	-1.4 (1)	[1097] (15)	182 (13)	1.14 (0.16)	[-60]
	0.0 (1)	[1090] (17)	184 (16)	0.93 (0.15)	[-67]
	1.4 (1)	[1116] (20)	194 (18)	0.90 (0.17)	[-41]
	2.8 (1)	[1125] (16)	178 (16)	0.87 (0.14)	[-32]
	4.2 (1)	1172 (19)	171 (18)	0.88 (0.16)	15
	6.3 (2)	1163 (20)	169 (20)	0.88 (0.17)	6
	9.8 (3) SW	1165 (40)	153 (41)	0.50 (01.7)	8

TABLE 2—*Continued*

Object	R (n) (arc sec)		cz [a,b] (km/s)	σ [a] (km/s)	γ	V [a,b] (km/s)
NGC 4062 (major axis, Vo=755 km/s)						
	-54.6 (8)	SE	892 (27)	89 (31)	0.58 (0.14)	137
	-44.8 (5)		876 (23)	98 (26)	0.81 (0.18)	121
	-37.8 (5)		796 (31)	96 (35)	0.63 (0.19)	41
	-30.8 (5)		804 (22)	<50	0.66 (0.15)	49
	-23.8 (5)		812 (20)	<50	0.62 (0.13)	57
	-16.8 (5)		823 (18)	53 (25)	0.72 (0.13)	68
	-11.2 (3)		822 (24)	70 (31)	0.63 (0.15)	67
	-7.0 (3)		790 (19)	91 (22)	0.81 (0.15)	35
	-3.5 (2)		807 (12)	<50	0.80 (0.10)	52
	-1.4 (1)		783 (13)	73 (16)	0.96 (0.12)	28
	0.0 (1)		769 (11)	99 (13)	1.14 (0.13)	14
	1.4 (1)		748 (12)	118 (13)	1.28 (0.15)	7
	3.5 (2)		714 (12)	80 (14)	1.05 (0.12)	41
	7.0 (3)		712 (13)	<50	0.65 (0.08)	43
	16.8 (5)		720 (14)	<50	0.66 (0.10)	35
	23.8 (5)		699 (19)	...	0.44 (0.09)	56
	30.8 (5)		690 (27)	...	0.38 (0.11)	65
	37.8 (5)		630 (27)	155 (28)	0.88 (0.24)	125
	46.9 (8)		630 (18)	...	0.41 (0.08)	125
	69.3 (8)	NW	621 (27)	...	0.44 (0.13)	134

EXPLANATION OF COLUMNS

Col. (2).—R = distance from center of galaxy in arc seconds; n = number of scan lines averaged together; each scan line is 1.″4 wide.
Col. (3).—cz = heliocentric stellar line-of-sight velocity (1 standard deviation error estimate from the Fourier quotient technique is given in parentheses).
Col. (4).—σ = stellar line-of-sight velocity dispersion (1 standard deviation error estimate in parentheses).
Col. (5).—γ = stellar line-strength index (1 standard deviation error estimate in parentheses).
Col. (6).—V = rotational line-of-sight velocity ($cz - V_0$, where V_0 is the central velocity determined from the center of symmetry of the outer velocities).
[a] Values from Fourier quotient fit using HD 134385 (K1 III) as the template star for most of the galaxies. HD 127007 (F2 III) was used as the template for the outer parts of M82. Values of cz also used spectra from the center of the galaxy as template when this gave a good fit.
[b] Values in brackets are affected by beam bending.
[c] $R = 0$ in M82 is defined as the brightest knot just west of the central dust lane.
[d] R is the distance measured parallel to the major axis, not the true distance to the center. The true distance is $(R^2 + Y^2)^{1/2}$, where $Y = 12''$.

Tammann (1981), with the magnitudes altered by adopting $V_{LG} = 300 \sin l \cos b$ as the component arising from the motion of the Sun with respect to the Local Group.

a) NGC 3898 (Sab; $M = -21.0$; $1'' = 122$ pc)

NGC 3898 is dominated by the bulge throughout the region of our data. Our numerical experiments indicate that a constant bulge rotation of 75 ± 20 km s^{-1} convolved with the disk rotation curve (Rubin 1983) produces a good fit to the observations (dashed line in Fig. 1). Correction factors of 1.44 for the line-of-sight projection effect, and csc i for the inclination effect, raise the rotational space velocity of the bulge to only $V_{bulge}^{space} = 117$ km s^{-1}. This is well below the disk rotation of 201 km s^{-1} at R_{bulge}, where R_{bulge} is the radius at the 21 mag arcsec^{-2} B isophote. We have chosen R_{bulge} as a characteristic radius of the bulge because the extrapolated central surface brightness of most spiral galaxies is about 21.65 mag arcsec^{-2} (Freeman 1970; Boroson 1981). The light within the 21 mag arcsec^{-2} isophote should therefore be dominated by the bulge. The dispersion curve for NGC 3898 stays fairly flat at about 190 km s^{-1}, with a gradual decline in the outer regions.

The minor-axis rotation curve (Fig. 2) is affected by beam bending, but is consistent with little or no rotation. The dispersion curve shows a gradual decline. The difference in the dispersion gradients of the major and minor axes might provide some evidence for anisotropic velocities as discussed in a study by Kormendy and Illingworth (1983). However, our minor-axis data are too meager to address this point.

b) NGC 2841 (Sb; $M = -21.4$; $1'' = 66$ pc)

NGC 2841 should provide a good test for our mixing experiments, since both the bulge and disk contribute over 25% of the total light from $R = 12''$ to $R = 50''$ (0.8–3.3 kpc). Unfortunately, the disk rotation inside 60″ is poorly known. Westerbork observations (Bosma 1978) with a $51'' \times 65''$ beam show a central hole in H I with a diameter of 80″–90″. High-resolution optical spectra (Rubin and Thonnard 1984) reveal the innermost measurable Hα and [N II] at $R = 52''$. Assuming for the disk rotation a constant velocity of 260 km s^{-1} (the value at 52″), the numerical experiments show that a constant bulge rotation of $V_{bulge}^{los} = 70 \pm 30$ km s^{-1} is consistent with the observations. V_{bulge} is quite uncertain in this galaxy because of the uncertainty in the disk velocity and also because of the lack of an obvious plateau in the stellar rotation curve. Correction factors increase the velocity of the bulge to $V_{bulge}^{space} = 111$ km s^{-1}, well below the emission-line velocity.

The velocity minimum at about 13″ appears to be real because it is seen clearly on both sides of the nucleus. The

TABLE 3

COMPARISONS WITH OTHER MEASUREMENTS

Galaxy and Axis	Type of Lines	Our[a] Central cz (km s^{-1})	Other Central cz (km s^{-1})	Our[b] σ_0 (km s^{-1})	Other σ_0 (km s^{-1})
NGC 2841:[c]					
Major	absorption	585	635	215(9)	229(14)
Minor	absorption	632	...	209(10)	...
		av. 608		av. 212	
NGC 2998:[c,d]					
Major	emission	4770	4767	...	...
Major	absorption	4760	4785	60(18)	107(24)
		av. 4765	av. 4776		
M82:[e,f]					
Major	emission	...	197	...	...
Major	absorption	180	195	...	...
			av. 196		
NGC 3200:[d]					
Major	emission	...	3516	...	...
	absorption	3518	...	...	...
		1175	1185	192(10)	219(16)
NGC 3898:[c,d]		1157	...	187(9)	...
Major	absorption				
Minor	absorption	av. 1166		av. 190	
		755	760	...	...
NGC 4062:[d]		755	...	...	...
Major	emission				
	absorption	av. 755			

NOTE.—Average difference of our repeats of the same galaxy: cz, absorption-absorption, 32 km s^{-1} ($n = 2$); cz, absorption-emission, 5 km s^{-1} ($n = 2$); σ_0, 6 km s^{-1} ($n = 2$). Comparison with other measurements (using averages of both emission and absorption): cz, -13 ± 10 km s^{-1} ($n = 6$); σ_0: -31 ± 15 km s^{-1}, a factor of 1.33 ($n = 3$), or a factor of 1.13 before applications of resolution-width correction to our data.

[a] Average of outer parts of rotation curves, except NGC 3200, where the value at the center is used.

[b] Average of three central scans.

[c] Central absorption-line velocity and velocity dispersion from Schechter 1983.

[d] Central emission-line velocity from Rubin *et al.* 1982.

[e] Average central emission-line velocity of Gottesman and Weiliachew 1977 and O'Connell and Mangano 1978.

[f] Central absorption-line velocity from Saito and Sasaki 1984.

suspicion that the beam-bending problem could somehow cause it seems unfounded, since the characteristic velocity separation has disappeared by 8″. Also, no similar effect is observed in the two other cases where beam bending is apparent. The velocity decrease is just marginally faster than Keplerian, which Lake and Norman (1983) have shown to be a diagnostic of a non-axisymmetric potential. A similar velocity decrease is seen in NGC 3945, a barred spiral with a clearly triaxial bulge (Kormendy 1982).

The dispersion curve (Fig. 1*b*) falls rapidly from a central value of 215 km s^{-1} to about 120 km s^{-1} at 20″. Beyond this point the dispersion rises slightly and then falls again. This rapid decline is not the result of contamination from light from the disk. The mixture of light from components at different systemic velocities will actually increase the dispersion over much of the galaxy (see dashed line in Fig. 1*b*). The true declines in the dispersion curves are therefore slightly steeper than observed.

The minor axis is severely affected by beam bending. However, the rotational velocities are compatible with very little or no rotation, while the dispersion curve again shows a decline, from 220 to 150 km s^{-1} at 20″.

c) NGC 4062 (Sc; $M = -19.5$; $1'' = 74$ pc)

There is a surprisingly sharp discontinuity in the absorption-line rotation curve of NGC 4062 at about 35″ (2.6 kpc). Here a well-defined plateau at $V = 55$ km s^{-1} jumps to a value $V = 125$ km s^{-1}, matching the rotational velocity of the disk. We might expect this to mark the transition point between the disk and the bulge. However, this discontinuity appears to be well beyond $R_{\rm bulge}$, which we estimate at about 5″ from glass copies of the Palomar Sky Survey. We have chosen not to estimate the bulge rotation in this galaxy because of the uncertainty in the true extent of the bulge. In the outer region where the disk dominates, the rotation curves of the stellar and gas components are in very good agreement.

The dispersion curve shows a rapid decline from a central value of 97 km s^{-1} to less than 50 km s^{-1} by about 10″. This continues a trend for the smaller bulge galaxies to have more rapid declines in their dispersion curves. In the outer region the

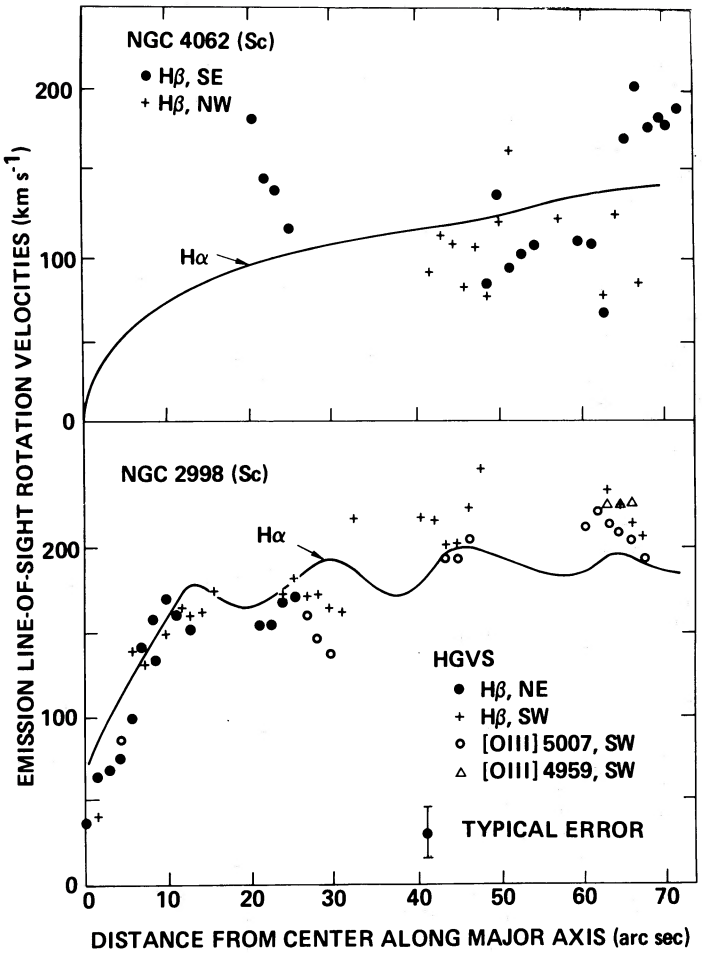

FIG. 4.—A comparison of emission line-of-sight rotation curves for NGC 4062 and NGC 2998 from HGVS observations and from high-resolution Hα observations (Rubin, Ford, and Thonnard 1980).

velocity dispersion is apparently broadened by the mixture of light from both the bulge and disk, again suggesting that the bulge dominates out farther than our estimate of $R_{\rm bulge}$ would suggest.

The emission-line rotation curve shown in Figure 4 is in rough agreement with Rubin, Ford, and Thonnard (1980) but shows more scatter. This results principally from the poorer spectral resolution of our observations (3.4 Å for this study as opposed to 1 Å for the Rubin, Ford, and Thonnard 1980 study).

d) NGC 2998 (Sc; $M = -22.8$; $1'' = 465$ pc)

NGC 2998 has a stellar velocity curve that lies below the gas rotation curve in the inner regions, but then quickly rises to match the gas velocities. The galaxy has a very small bulge, so the disk becomes dominant quite near the center. An estimate of the bulge rotation is not possible from our data. The agreement between emission and absorption velocities in the outer regions of both NGC 2998 and NGC 4062 is reassuring, since it is expected that both the gas and stars in the disk have the same rotational velocities.

The flat rotation curves from emission lines in disks of spiral galaxies are one important piece of evidence for the existence of massive dark halos around spirals. It would be valuable to establish that absorption-line rotation curves in spiral disks offer the same evidence. Unfortunately, only for NGC 4062 and NGC 2998 have we determined absorption-line rotation curves that are clearly dominated by the disk (Fig. 1), and these only reach 55% and 30% of the extent of the emission-line velocities, respectively. Hence the absorption-line velocities offer no new constraints on the halo mass distribution, even though they agree with the emission-line velocities in the region of overlap.

The very low value of σ is consistent with the small bulge. The dispersion curve does not extend far enough to include in our analysis.

The emission-line rotation curve shown in Figure 4 is in fairly good agreement with the photographic emission-line rotation curve of Rubin, Ford, and Thonnard (1980), but again shows larger scatter as a result of the poorer spectral resolution. Our velocity gradient is not as steep in the central region, because of the wider slit (2.″4 vs. 1.″3) and the poorer seeing conditions.

e) NGC 3200 (Sab; $M = -22.9$; $1'' = 322$ pc)

NGC 3200 has very weak absorption lines, so only a central measurement has been determined. The value of $\sigma_0 = 138 \pm 20$ has been obtained by adding the central six scans together to improve the signal, and is typical for an average-sized bulge.

f) M82 (I; $M = -18.6$; $1'' = 18$ pc)

We have obtained the absorption-line velocities along the principal plane of the peculiar galaxy M82, and have measured velocities in the region where the emission lines do not contaminate the absorption. Figure 5 shows that the rotational velocities are falling slightly in the outer regions. However, because of the presence of large amounts of dust in this edge-on galaxy, it is not clear to which region within the galaxy the observations correspond. Stellar velocities in M82 have also been measured by Saito and Sasaki (1984). At the extremes of their measurements ($R = 40''$) velocities are ± 75 km from the central velocity, in fair agreement with our more extensive observations. No measurement of the velocity dispersion is possible because the dust obscures any obvious bulge component. Because of these problems, M82 has been excluded from the ensuing discussion.

Most previous studies of the dynamics of M82 (e.g., O'Connell and Mangano 1978) have considered exclusively the disordered velocity field of the excited gas. Our stellar velocities show a more uniform velocity field with the main component rotating like a fairly normal disk. Declines in rotational velocities are almost never seen in spiral galaxies, but are typical of interacting galaxies (Rubin and Ford 1983). If this decline is real and not an artifact of obscuration by dust, it may indicate that much of the outer mass has been removed from M82. Recently, Schweizer, Whitmore, and Rubin (1983) have suggested that M82 may be in the process (or may have failed in the attempt) of forming a polar ring from material obtained during an encounter with M81. Perhaps this encounter has also stripped off the outer halo of M82.

IV. DISCUSSION

a) $V^{\rm los}_{\rm bulge}/\sigma_0$ versus Bulge Ellipticity

Is a spiral bulge just an elliptical galaxy with a disk? Whitmore, Kirshner, and Schechter (1979), Whitmore and Kirshner (1981), and KI find that spiral bulges exhibit essentially the

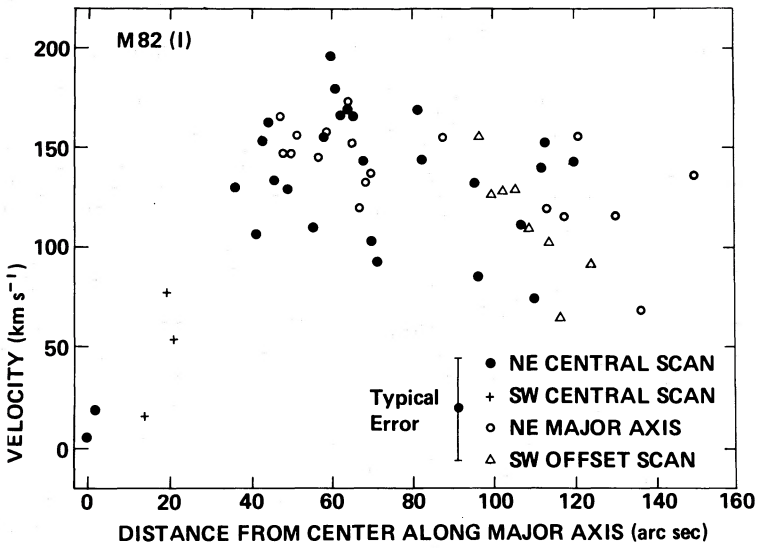

FIG. 5.—Stellar rotation curve for M82. The presence of large amounts of dust in this edge-on galaxy make it uncertain where within the galaxy the rotation is being measured.

same relation between bulge luminosity and central velocity dispersion as do elliptical galaxies. This suggests that the two systems have similar dynamics. However, KI found that spiral bulges rotate faster than ellipticals. It now appears that this apparent difference was caused by comparing small bulges with large ellipticals. Davies *et al.* (1983) find that small ellipticals, with sizes more characteristic of spiral bulges, exhibit rotational velocities that are comparable to those of spiral bulges.

To compare the relative amounts of dynamical support provided by rotation and velocity dispersions, we evaluate V^{los}_{bulge}/σ_0, where V^{los}_{bulge} is the line-of-sight rotational velocity of the bulge at R_{bulge}, and σ_0 is the line-of-sight central velocity dispersion. We average the central three values of the dispersion to obtain our value of σ_0 in order to reduce our uncertainties. Values of V^{los}_{bulge} and σ_0 are found in Table 4.

Figure 6 plots V^{los}_{bulge}/σ_0 against ellipticity for the spiral bulges studied here and in KI. We make visual estimates of the ellipticities. The line represents models of oblate galaxies with isotropic velocities superimposed on a global rotation (Binney 1980). The shape of these model galaxies is determined by a balance between the dynamical support from rotation and from the dispersion. The spiral bulges fall well below the isotropic rotator models.

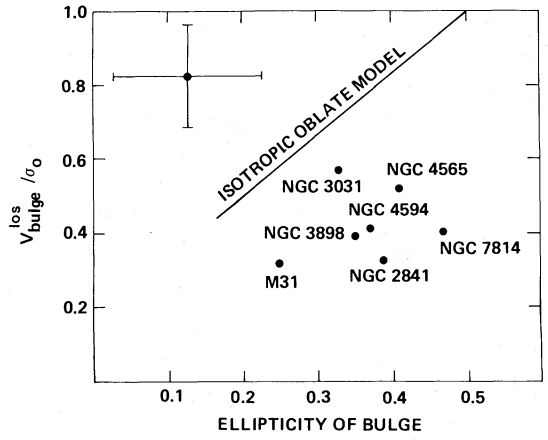

FIG. 6.—V^{los}_{bulge}/σ_0 vs. ellipticity for our galaxies and those of KI. The solid line shows where oblate, isotropic galaxies would fall on this diagram (Binney 1980). This line is actually for mean values of v and σ. However, Binney (1981) comments that, for his models at least, the ratio of peak values provides a good estimate of the ratio of mean values.

Our results are significantly different from those of KI, who conclude that the bulges of spiral galaxies could be explained by the isotropic models, even though most of their observed points also fall slightly below the model line. Several effects are responsible for this difference:

1. In the Binney models, the peak rotational velocity in the bulge generally occurs at a distance of about 5 core radii (R_c) from the center of the galaxy (Binney 1980). For elliptical galaxies, KI note that $5R_c$ occurs at about $\frac{1}{2}$ the effective radius (R_e). For spiral galaxies, where much of the total luminosity comes from the disk, $5R_c$ occurs at about $R_e/6$ for an Sb galaxy (using photometry from Boroson 1981). Our use of the 21 mag arcsec^{-2} isophote to define R_{bulge} results in an average value for R_{bulge} near $R_e/3$, or about $10R_c$, where Binney's models retain about 95% of their peak rotation. The KI values, however, were measured at about $1.5R_e$, or about $45R_c$. Here the models predict that rotation curves have fallen to about 75% of their peak values, in contrast to the KI data, which show the rotation is still rising at the last observed point. This means either that the Binney models are inappropriate for spiral bulges (and the apparent agreement in the V/σ vs. ellipticity diagram was due simply to a fortuitous choice of where to measure the bulge rotation) or that the outer gradient in the rotation is caused by contamination by the rapidly rotating disk. In either case the KI measurements cannot be taken as agreement with the Binney models.

2. Binney (1981) advocates the use of central velocity dispersions as the best determination of the velocity dispersion to compare with rotational velocities. KI use a mean of dispersions measured to $R_e/2$. Moreover, they exclude the central 1".4, which they believe may be deviant because of interaction with the nucleus. However, there is no evidence in our data, or in KI, that the central 1".4 is abnormal. The exclusion of the

TABLE 4

PROPERTIES OF THE BULGE AND THE DISK

Galaxy (1)	Type (2)	Ellipticity of Bulge (3)	R_{bulge} (arcsec), R_{bulge} (kpc), and $\frac{R_{bulge}}{R_{25}}$ (4)	Inclination of Disk (deg) (5)	Distance (Mpc) (6)	σ_0, $\langle\sigma\rangle$, and σ_{bulge} (km s^{-1}) (7)	$\frac{\sigma_{bulge}}{\sigma_0}$ and $\frac{\langle\sigma\rangle}{\sigma_0}$ (8)	V^{los}_{bulge} and V^{space}_{bulge} (km s^{-1}) (9)	V_{max} and V_{disk} (km s^{-1}) (10)	$\frac{V^{los}_{bulge}}{\sigma_0}$ (11)	$\frac{V^{space}_{bulge}}{V_{disk}}$ and $\frac{V^{space}_{bulge}}{V_{max}}$ (12)	$\frac{V_{max}}{\sigma_0}$ (13)
M31.....	Sb	0.25	390 1.2 0.07	77	0.65	160 126 116	0.72 0.79	51 75	273 180	0.32	0.42 0.27	1.71
NGC 2841	Sb	0.39	32 2.1 0.13	65	13.5	215 169 134	0.62 0.79	70 111	309 309	0.33	0.36 0.36	1.44
NGC 2998	Sc	...	... ...	62	95.6	60	... ...	... ...	213 ...	...	... ...	3.55
NGC 3031	Sab	0.33	80 1.3 0.10	59	3.3	159 146 133	0.84 0.92	90 151	300 300	0.57	0.50 0.50	1.53
NGC 3200	Sab	...	... ...	72	65.3	138	... ...	... ...	285 ...	...	... ...	2.07
NGC 3898	Sab	0.35	18 2.0 0.14	67	23.1	192 197 176	0.92 1.03	75 117	269 201	0.39	0.58 0.43	1.40
NGC 4062	Sc	0.40	5 0.4 0.04	64	15.1	97 84 ...	0.70 0.87	... ...	162 61	...	... ...	1.67
NGC 4565	Sb	0.41	36 3.3 0.07	90	18.9	161 136 102	0.63 0.84	84 121	246 246	0.52	0.49 0.49	1.53
NGC 4594	Sa	0.37	48 4.5 0.18	84	19.3	216 224 221	0.98 1.03	89 129	345 300	0.41	0.43 0.37	1.60
NGC 7814	Sab	0.47	21 2.5 0.11	90	25.0	168 164 138	0.82 0.98	68 98	246 ...	0.40	... 0.40	1.46
										av. 0.42 ± 0.09	av. 0.46 ± 0.08 0.40 ± 0.08	

EXPLANATION OF SELECTED COLUMNS

NOTE.—Where more than one quantity is indicated by the column heading, the indicated values are listed vertically in the column.

Col. (2).—Galaxy types from de Vaucouleurs, de Vaucouleurs, and Corwin 1976.

Col. (3).—Ellipticities from KI, except NGC 2841, NGC 3898, and NGC 4062, which are from our visual estimates from the *Hubble Atlas* (Sandage 1961). R_{25} is the blue radius at the 25 mag arcsec^{-2} isophote from de Vaucouleurs, de Vaucouleurs, and Corwin 1976.

Col. (4).—R_{bulge} is the major-axis radius at an isophotal blue radius of 21 mag arcsec^{-2} from: M31—Hodge and Kennicutt 1982; NGC 2841—Whitmore and Kirshner 1982; NGC 3031—Schweizer 1976; NGC 3898 and NGC 4594—Boroson 1981; NGC 4062—visual estimate of glass copy of Palomar Sky Survey; NGC 4565—minor-axis profile of Kormendy and Bruzual 1978; NGC 7814—minor-axis profile of van Houten 1961. Major-axis radii were estimated from the minor-axis profiles by using the ellipticities.

Cols. (5) and (10).—Inclination of the disk and emission-line velocities from: M31—Roberts and Whitehurst 1975; NGC 2841—Rubin and Thonnard 1984; NGC 2998 and NGC 4062—Rubin, Ford, and Thonnard 1980; NGC 3031—Goad 1976; NGC 3200—Rubin *et al.* 1982; NGC 3898—Rubin 1983; NGC 4565—Bosma 1978; NGC 4594—Schweizer 1978; NGC 7814—H I width from Whitmore and Kirshner (1981). V_{max} is the maximum emission-line velocity in the plane of the galaxy. V_{disk} is the emission-line velocity in the plane of the galaxy at R_{bulge}.

Col. (6).—Distances from the source used for emission-line velocities or from KI when available.

Col. (7).—σ_0 is the average of the three values of the dispersion closest to the center for our data and KI's data. $\langle\sigma\rangle$ is the average value of the dispersion out to R_{bulge}. Note that values from KI are from scans which were parallel to the major axis, but offset from the nucleus. σ_{bulge} is the average of the dispersions for the four values closest to R_{bulge}. Values < 50 km s^{-1} were taken as 50 km s^{-1}. For NGC 3031, σ_{bulge} is calculated from $(2\langle\sigma\rangle/\sigma_0) - 1$, with values of $\langle\sigma\rangle$ and σ_0 from Davies *et al.* 1983.

Col. (9).—V^{los}_{bulge} is the stellar line-of-sight rotation along the major axis of the bulge, corrected for mixing with disk light using numerical experiments, or by multiplying by 0.90 for M31 and NGC 3031 where contamination from disk light is likely. The KI correction for off-axis scans is also made where appropriate. V^{space}_{bulge} is V^{los}_{bulge} corrected for line-of-sight projection effects by multiplying by 1.44, and corrected for inclination by multiplying by csc i.

central values by KI, and their use of mainly off-center scans at large radii where the velocity dispersion is smaller, result in smaller values for the velocity dispersion.

Binney (1981) comments that, for his models at least, the ratio of the peak values provides a good estimate of the ratio of the mean values. A comparison with these models therefore requires that both V and σ be either mean values or peak values. By mixing the two, KI make an unfair comparison with the models. While it would be preferable to use mean values to compare directly with the tensor virial theorem (Binney 1978), we have chosen to use peak values because they are much better defined. A true measurement of the mean values would require observations throughout the bulge (not just far from the nucleus as in KI) and a weighting by luminosity (requiring an accurate luminosity profile and bulge decomposition).

3. The determination of bulge ellipticity is more uncertain than is generally believed. For example, Hodge and Kennicutt (1982) show that in M31 the ellipticity is a rapidly changing function of radius with no hint of a plateau in the region of importance. They find a value for the ellipticity of 0.1 at 2′, increasing to 0.4 at 6′ (where the bulge still dominates over the disk by a factor of 3). A visual estimate from the *Hubble Atlas* (Sandage 1961) yields a value for the ellipticity of 0.38, rather than 0.25 ± 0.03 as used by KI. This would move M31 farther from the isotropic rotator models.

Another example is NGC 3379, where Davies and Illingworth (1983) use an ellipticity of 0.13 ± 0.02. However, in § Vc they suggest that an ellipticity of 0.05 measured within 3 core radii is more relevant. This would bring NGC 3379 into agreement with the rotationally flattened oblate speroid models.

4. There is no correction for contamination by disk light in KI. While most of their spectra are taken above the plane of edge-on galaxies, this is not true for M31 and M81. We have therefore lowered $V_{\rm bulge}$ by 10% in these galaxies.

We also wish to emphasize that the Binney models are for elliptical galaxies with constant values of M/L. For spiral bulges, both the varying of M/L with radius and the likely influence of the disk potential should be taken into account.

With all these factors in mind, we believe that the conclusion by KI that spiral bulges are isotropic oblate rotators is premature, and that anisotropic velocities are likely to be important.

b) $V^{\rm space}_{\rm bulge}/V_{\rm disk}$

A primary goal of this study is to compare the rotation of the bulge ($V^{\rm space}_{\rm bulge}$) with the rotation of the disk ($V_{\rm disk}$ or $V_{\rm max}$ at the peak of the emission-line rotation curve). In Table 4 we have collected rotational velocities for the disks of spiral galaxies with known values of the bulge rotation. At $R_{\rm bulge}$ the average value of $V^{\rm space}_{\rm bulge}/V_{\rm disk}$ is 0.46 ± 0.08, while $V^{\rm space}_{\rm bulge}/V_{\rm max} = 0.40 \pm 0.08$. When this value of $V^{\rm space}_{\rm bulge}/V_{\rm max}$ is used with $V_{\rm max}$ to predict $V^{\rm space}_{\rm bulge}$, we find a standard deviation in the residual of 22 km s^{-1}. We can therefore predict $V^{\rm space}_{\rm bulge}$ with errors of about 20%. We should note that an important systematic error is possible because of the use of the 1.44 correction factor to correct the line-of-sight values to the space velocities (see § II). This value is for a very simple model. It is quite possible that the correction is in error by as much as 20%. This would increase our estimated uncertainty in $V^{\rm space}_{\rm bulge}/V_{\rm disk}$ to 0.11.

c) *Implications for the Formation of Spiral Galaxies*

The low values of $V^{\rm space}_{\rm bulge}/V_{\rm disk}$ can be used to constrain the theories for the formation of spiral galaxies. If the stars in the bulge originally formed in the outer regions of a galaxy and then collapsed to the present configuration, conservation of angular momentum would require a large increase in the rotational velocity of the bulge. If both the bulge and the disk stars originated in the same region with the same rotational velocities, we would expect the bulge to rotate much faster than the disk, since it collapsed to a smaller radius. We would also expect small bulges to rotate faster than large bulges. The observations contradict these predictions.

An alternative possibility is that stars in the bulge formed at about their present radii. For example, clouds with high angular momentum would tend to stay in the outer parts of a galaxy. Clouds with low angular momentum, converging toward the center, would collide, resulting in frequent star formation. Stars formed from this low-angular-momentum material might tend to have radial orbits.

Yet another possibility is that a collapse of the protogalaxy might result in rapid star formation near the center where the density is highest. This might also produce orbits that are more radial than isotropic (Tonry 1983).

d) *The Decline in the Dispersion Gradient*

Rotation curves of most spiral galaxies are flat or slightly rising, so the dominant massive component is often assumed to be an isothermal sphere. If stars in the bulges of spiral galaxies have isothermal and isotropic velocity dispersion tensors, the dispersion curves should also be flat. However, most spiral bulges in our sample have falling dispersion curves, with the later Hubble types having the fastest decline. This is shown in Figure 7.

One possible explanation for this decline is the decoupling of the bulge and halo found by Whitmore, Kirshner, and Schechter (1979) and Whitmore and Kirshner (1981). If the velocity dispersion in the bulge of a spiral galaxy is the same as the velocity dispersion of the halo, the value of $V_{\rm max}/\sigma_0$ should be about 1.4 (Gott 1977). This appears to be the case for large bulge systems. However, for small bulge spirals the value of $V_{\rm max}/\sigma_0$ is generally greater than 2, indicating that the bulge has decoupled from the halo and is now a distinct dynamical component. Our current data also support this conclusion: the smallest bulge system (NGC 2998) has $V_{\rm max}/\sigma_0 = 3.6$, while the average of the two largest bulge systems (NGC 4594 and NGC 7814) has $V_{\rm max}/\sigma_0 = 1.5$.

If the smaller bulges are separate from the halo, they could

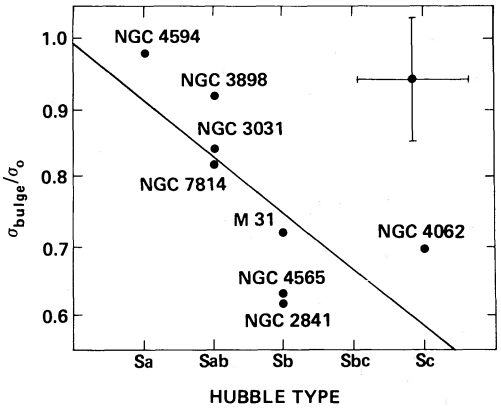

FIG. 7.—$\sigma_{\rm bulge}/\sigma_0$ vs. Hubble type, using data from Table 4. The line is a least squares fit with Hubble type as the independent variable. The correlation coefficient is 0.73.

dominate the mass distribution in the inner region while the dark halo dominates in the outer region. The bulge could then show a decline in the dispersion profile similar to most constant M/L models of spheroidal systems. This might explain why the small bulge systems show more of a dispersion gradient than the large bulge systems.

Another possible contribution to this decline might result if the stars in the bulge have fairly radial orbits, as suggested in the previous section. The decline in the dispersion curves could then be caused by projection effects. At the center of the galaxy we would observe nearly the full velocity dispersion of the stars, since orbits of most stars would be aligned with our line of sight. Farther out along the slit the star's orbits would be seen projected at various angles to our line of sight, but never exactly toward us. The integration of all these orbits would result in a lower measurement of the dispersion in the outer regions (see Tonry 1983 for an example).

The possibility that radial orbits might be prevalent in spiral bulges is also suggested in a study by Schechter, Whitmore, and Rubin (unpublished). They show that if isotropic velocities are assumed for the bulge stars, the estimated mass of the bulge exceeds the total mass in the inner regions inferred from the disk rotation. One likely explanation for this would be radial orbits, since the velocities of stars on radial orbits are not indicative of the mass near the center. These stars build up most of their velocity in the outer regions and simply drift through the center at nearly constant speed, whether there is much mass there or not. Tremaine and Ostriker (1982) use this fact to construct a model for the nucleus of M31 that has no mass. Tonry (1983) has also developed models of ellipticals with largely radial orbits.

More evidence for radial orbits in bulges comes from Woolley (1978), using RR Lyrae stars in the solar neighborhood, and from Pier (1984), using halo field stars. They both find velocity ellipsoids aligned with the galactic center, with ratios of $R^2:\Theta^2:\Phi^2$ of about 3:2:1, where R is the radial component, Θ is the azimuthal component, and Φ is the meridional component.

An interesting question is whether elliptical galaxies show any trend for low-luminosity objects to have steeper velocity dispersion gradients. An examination of 11 low-luminosity ellipticals observed by Davies *et al.* (1983) does not show an analogous trend to the spiral bulges. This would suggest an intrinsic difference between spiral bulges and elliptical galaxies. However, because of the small number of galaxies both in our sample ($n = 8$) and in that of Davies ($n = 11$), caution must be exercised in interpreting the difference.

V. SUMMARY

We have obtained kinematical data for several spiral bulges with the purpose of constructing an evolutionary picture that is consistent with the properties of both the bulge and the disk. Some specific conclusions are the following.

1. The intrinsic rotational velocities in the bulges of spiral galaxies can be determined by performing numerical experiments on spectra with contributions from both the disk and the bulge components. Differences in both the line strengths and the velocity dispersions must be considered. Accurate luminosity profiles are also required for most cases.

2. In the region where the disk dominates, the stellar rotation matches the gas rotation.

3. Along the major axis, spiral bulges rotate with velocities that are about 50% of the disk rotational velocities at the same radius, and 40% of the maximum rotation velocity of the disk. These observations are not compatible with models in which stars in the bulge form at large radii and then collapse to their present configuration. We suggest that the bulge stars in late-type spirals formed near the center, perhaps from the collision of low-angular-momentum gas clouds or the collapse of the protogalaxies. Both of these mechanisms might produce velocity ellipsoids that are extended in the radial direction.

4. The dispersion curves of most spiral galaxies show a decline with radius in the bulge. This decline is largest in small bulge systems. This might indicate that small bulges are decoupled from the halo, that bulge stars have fairly radial orbits, or some combination of the two.

5. A reevaluation of the $V^{\rm los}_{\rm bulge}/\sigma_0$ versus ellipticity diagram for spiral bulges shows that the observations are not in agreement with models of isotropic oblate galaxies, contrary to the conclusions of KI.

We would like to thank Drs. D. McElroy and G. Illingworth for help in using the HGVS and in performing the preliminary reductions at KPNO, and P. Schechter, D. Burstein, and an anonymous referee for valuable correspondence. Part of this work was performed while B. C. W. was at Arizona State University.

REFERENCES

Binney, J. 1978, *M.N.R.A.S.*, **183**, 501.
———. 1980, *M.N.R.A.S.*, **190**, 421.
———. 1981, in *The Structure and Evolution of Galaxies*, ed. S. M. Fall and D. Lynden-Bell (Cambridge: Cambridge University Press), p. 55.
Boroson, T. 1981, *Ap. J. Suppl.*, **46**, 177.
Bosma, A. 1978, Ph.D. thesis, University of Groningen.
Davies, R. L., Efstathiou, G., Fall, S. M., Illingworth, G., and Schechter, P. L. 1983, *Ap. J.*, **266**, 41.
Davies, R. L., and Illingworth, G. 1983, *Ap. J.*, **266**, 516.
de Vaucouleurs, G., de Vaucouleurs, A., and Corwin, H. R. 1976, *Second Reference Catalogue of Bright Galaxies* (Austin: University of Texas Press).
Ford, W. K., and Whitmore, B. C. 1982, *Carnegie Yrb.* (Washington: Carnegie Institution of Washington), p. 580.
Freeman, K. C. 1970, *Ap. J.*, **160**, 811.
Goad, J. W. 1976, *Ap. J. Suppl.*, **32**, 89.
Gott, J. R. 1977, *Ann. Rev. Astr. Ap.*, **15**, 235.
Gottesman, S. T., and Weiliachew, L. 1977, *Ap. J.*, **211**, 47.
Hodge, P. W., and Kennicutt, R. C. 1982, *A.J.*, **87**, 264.
Illingworth, G., and Schechter, P. 1982, *Ap. J.*, **256**, 481.
Kormendy, J. 1977, *Ap. J.*, **217**, 406.
———. 1982, *Ap. J.*, **257**, 75.
Kormendy, J., and Bruzual, A. 1978, *Ap. J. (Letters)*, **223**, L63.
Kormendy, J., and Illingworth, G. 1982, *Ap. J.*, **256**, 460 (KI).
———. 1983, *Ap. J.*, **265**, 632.
Lake, G., and Norman, C. 1983, *Ap. J.*, **270**, 51.
McElroy, D. B. 1983, *Ap. J.*, **270**, 485.
O'Connell, R. W., and Mangano, J. J. 1978, *Ap. J.*, **221**, 62.
Pier, J. 1984, *Ap. J.*, **281**, 260.
Roberts, M. S., and Whitehurst, R. N. 1975, *Ap. J.*, **201**, 327.
Rubin, V. C. 1983, in *IAU Symposium 100, Internal Kinematics and Dynamics of Galaxies*, ed. E. Athanassoula (Dordrecht: Reidel), p. 1.
Rubin, V. C., Burstein, D., Ford, W. K., and Thonnard, N. 1984, *Ap. J.*, in press.
Rubin, V. C., and Ford, W. K. 1983, *Ap. J.*, **271**, 556.
Rubin, V. C., Ford, W. K., and Thonnard, N. 1980, *Ap. J.*, **238**, 471.
Rubin, V. C., Ford, W. K., Thonnard, N., and Burstein, D. 1982, *Ap. J.*, **261**, 439.
Rubin, V. C., and Thonnard, N. 1984, in preparation.
Saito, M. and Sasaki, M. 1984, *Pub. Astr. Soc. Japan*, **36**, 305.
Sandage, A. 1961, *The Hubble Atlas of Galaxies* (Washington: Carnegie Institution of Washington).
Sandage, A., and Tammann, G. A. 1981, *A Revised Shapley-Ames Catalog of Bright Galaxies* (Washington: Carnegie Institution of Washington).
Sargent, W. L. W., Schechter, P. L., Boksenberg, A., and Shortridge, K. 1977, *Ap. J.*, **212**, 326.
Schechter, P. L. 1983, *Ap. J. Suppl.*, **52**, 425.

Schweizer, F. 1976, *Ap. J. Suppl.*, **31**, 313.
———. 1978, *Ap. J.*, **220**, 98.
Schweizer, F., Whitmore, B. C., and Rubin, V. C. 1983, *A.J.*, **88**, 909.
Tonry, J. L. 1983, *Ap. J.*, **266**, 58.
Tremaine, S., and Ostriker, J. P. 1982, *Ap. J.*, **256**, 435.
van Houten, C. J. 1961, *Bull. Astr. Inst. Netherlands*, **16**, 1.
Whitmore, B. C. 1980, *Ap. J.*, **242**, 53.
Whitmore, B. C., and Kirshner, R. P. 1981, *Ap. J.*, **250**, 43.
———. 1982, *A.J.*, **87**, 500.
Whitmore, B. C., Kirshner, R. P., and Schechter, P. L. 1979, *Ap. J.*, **234**, 68.
Woolley, R. 1978, *M.N.R.A.S.*, **184**, 311.
Young, P., Sargent, W. L. W., Boksenberg, A., Lynds, C. R., and Hartwick, F. D. A. 1978, *Ap. J.*, **222**, 450.

W. K. FORD and V. C. RUBIN: Department of Terrestrial Magnetism, Carnegie Institution of Washington, 5241 Broad Branch Road, N.W., Washington, DC 20015

B. C. WHITMORE: Space Telescope Science Institute, 3700 San Martin Drive, Baltimore, MD 21218